Published in final edited form as:

ACS Nano. 2018 March 27; 12(3): 2466–2473. doi:10.1021/acsnano.7b08152.

Core–Shell Microneedle Gel for Self-Regulated Insulin Delivery

Jinqiang Wang[†,‡,⊥], **Yanqi Ye**[†,‡,⊥], **Jicheng Yu**[†,‡], **Anna R. Kahkoska**[§], **Xudong Zhang**[†,‡], **Chao Wang**[†,‡], **Wujin Sun**[†,‡], **Ria D. Corder**[‖], **Zhaowei Chen**[†,‡], **Saad A. Khan**[‖], **John B. Buse**[§], and **Zhen Gu**[*,†,‡,§]

[†] Joint Department of Biomedical Engineering, University of North Carolina at Chapel Hill and North Carolina State University, Raleigh, North Carolina 27695, United States

[‡] Division of Molecular Pharmaceutics and Center for Nanotechnology in Drug Delivery, Eshelman School of Pharmacy, University of North Carolina at Chapel Hill, Chapel Hill, North Carolina 27599, United States

[§] Department of Medicine, University of North Carolina School of Medicine, Chapel Hill, North Carolina 27599, United States

[‖] Department of Chemical and Biomolecular Engineering, North Carolina State University, Raleigh, North Carolina 27695, United States

Abstract

A bioinspired glucose-responsive insulin delivery system for self-regulation of blood glucose levels is desirable for improving health and quality of life outcomes for patients with type 1 and advanced type 2 diabetes. Here we describe a painless core–shell microneedle array patch consisting of degradable cross-linked gel for smart insulin delivery with rapid responsiveness and excellent biocompatibility. This gel-based device can partially dissociate and subsequently release insulin when triggered by hydrogen peroxide (H_2O_2) generated during the oxidation of glucose by a glucose-specific enzyme covalently attached inside the gel. Importantly, the H_2O_2-responsive microneedles are coated with a thin-layer embedding H_2O_2-scavenging enzyme, thus mimicking the complementary function of enzymes in peroxisomes to protect normal tissues from injury caused by oxidative stress. Utilizing a chemically induced type 1 diabetic mouse model, we demonstrated that this smart insulin patch with a bioresponsive core and protective shell could effectively regulate the blood glucose levels within a normal range with improved biocompatibility.

Abstract

[*]Corresponding Author zgu@email.unc.edu.

[⊥]These authors contributed equally to this work. J.W., Y.Y., J.B., and Z.G. designed the experiments. J.W., Y.Y., J.Y, X.Z., C.W, R.C., Z.C, W.S., and S.K. performed experiments and collected data. J.W., Y.Y., A.K., J.B., and Z.G. analyzed the data and wrote the paper

ASSOCIATED CONTENT

Ⓢ Supporting Information

The Supporting Information is available free of charge on the ACS Publications website at DOI: 10.1021/acsnano.7b08152. Experimental details and data (PDF)

Notes

The authors declare no competing financial interest.

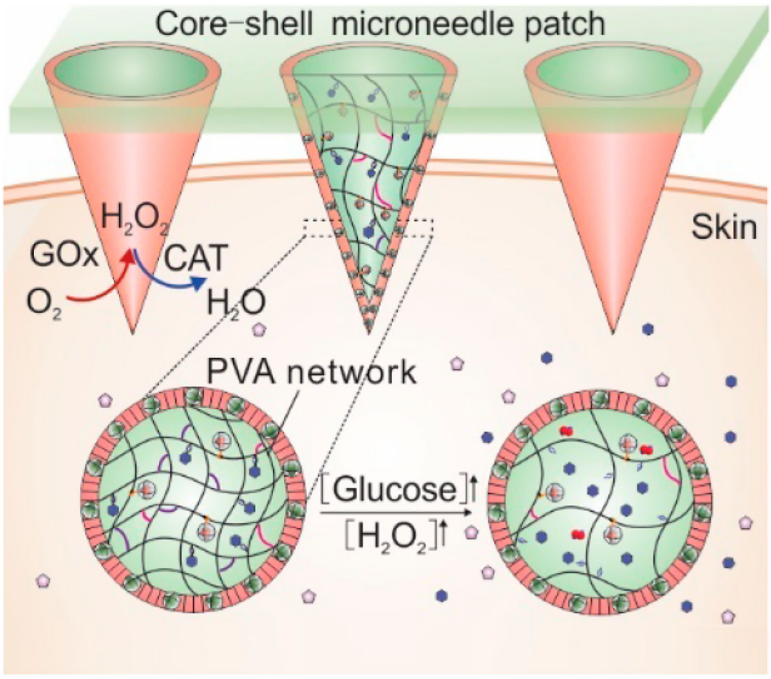

Keywords

microneedle; stimuli-responsive; diabetes; drug delivery; hydrogel

Diabetes mellitus, a chronic disease affecting 422 million people worldwide in 2016, is characterized by a deficit of endogenously produced insulin and elevated blood glucose levels (BGLs).[1,2] In the absence of proper control, chronically elevated BGLs can lead to limb amputation, blindness, kidney failure, and cardiovascular disease.[3] To prevent these diabetic complications, patients with type 1 and advanced type 2 diabetes use injected or infused insulin to achieve normoglycemia.[4] However, open-loop exogenous insulin injection or infusion generally fails to reach targets and carries the additional risk of hypoglycemia when insulin doses exceed that needed; these hypoglycemic episodes can be severe and even lethal.[3] Therefore, there is an urgent need for a bioinspired "artificial β-cell" system that can intelligently "secrete" desirable amounts of insulin in response to elevated BGLs while maintaining basal insulin release kinetics at normoglycemia. To this end, closed-loop device-based systems have been developed and integrate a patient-calibrated continuous glucose-monitoring sensor and an external insulin infusion pump.[5] However, such systems remain challenging regarding algorithm accuracy and sensor reliability.[6] Meanwhile, chemically engineered formulations or devices that can swell, degrade, or dissociate in response to ambient elevated BGLs have attracted increasing attention as an alternative solution.[7–11] These systems typically employ one of three different mechanisms of actions,[12,13] based on glucose oxidase (GOx),[8,9,10,14–20] phenylboronic acid (PBA),[21–26] and glucose binding proteins (GBP), respectively.[27–29] GOx catalyzes the oxidation of D-glucose to D-gluconolactone, which can hydrolyze to gluconic acid and generate hydrogen peroxide in the presence of oxygen:

$$glucose + O_2 + H_2O \xrightarrow{\text{GOx}} gluconicacid + H_2O_2$$

Accordingly, acidity-sensitive systems entrapping GO**x** can create a local acidic environment in response to elevated glucose levels to trigger the release of insulin. However, it is highly challenging to rapidly switch the physiological pH *in vivo* to achieve fast response[15]. We have previously developed a hypoxia-sensitive formulation to achieve a fast response, based on the enzymatic consumption of local oxygen level.[14] However, this formulation is limited by the hydrogen peroxide that remains in this system, raising concerns over long-term biocompatibility.[30] Moreover, the simultaneous release of GO**x** with insulin has the potential to cause systemic toxicity.[31] Moving forward, the next generation of smart insulin delivery should be developed to prioritize rapid responsiveness, ease of preparation and administration, and excellent biocompatibility.

Here, we report a core–shell microneedle (MN) array patch[32,33] consisting of degradable cross-linked poly(vinyl alcohol) (PVA) gel for self-regulated insulin delivery with rapid responsiveness to elevated BGLs. As shown in Figure 1a, the core component of this device contains GO**x** that generates H_2O_2 to stimulate the release of insulin, while the shell component is embedded with catalase (CAT) that serves as an active strainer to scavenge excessive H_2O_2, thus minimizing the risk of inflammation caused by H_2O_2 (Figure S1). To achieve H_2O_2-responsive insulin release, insulin is chemically modified with 4-nitrophenyl 4-(4,4,5,5-tetramethyl-1,3,2-dioxaborolan-2- yl) benzyl carbonate (designated insulin-NBC, Figure 1b) and subsequently anchored to the water-soluble PVA matrix.[34] Of note, to further facilitate transport of free insulin in the polymeric matrix and promote responsiveness speed, PVA is also gelated by an H_2O_2-labile linker: N^1-(4-boronobenzyl)-N^3- (4-boronophenyl)-N^1,N^1,N^3,N^3-tetramethylpropane-1,3-diaminium (TSPBA) (Figure 1c). Both insulin-NBC and TSPBA are oxidized and hydrolyzed when exposed to locally elevated levels of H_2O_2 generated by GO**x** at high glucose concentrations,[35,36] leading to the quick release of free insulin (Figure 1a). To limit the potentially harmful release of GO**x** itself,[31] GO**x** is encapsulated into the acrylated nanogel (GO**x**-NG) to acquire a large size[10] and get immobilized with covalent linkage to PVA methacrylate during radical polymerization, which forms a partially uncleavable network of PVA to further prevent the leakage of GO**x**-NG while maintaining ease of insulin release. The shell component is designed to mimic the complementary function in peroxisome[37] where catalase nanogel (CAT-NG)[10] is formed and embedded inside a cross-linked PVA layer covering the surface of PVA-TSPBA MN core. Collectively, the design of the core and shell components offers: (1) sufficient catalysis with GO**x** to perform the glucose-responsive action in the core and (2) efficient elimination of H_2O_2 to alleviate inflammation affecting the surrounding tissues and mitigate systemic toxicity. Additionally, the direct conjugation method that is utilized to load insulin onto the MN scaffold enhances both efficiency and capacity of the insulin-loading process. Upon painless transcutaneous administration, this bioresponsive MN patch partially dissolves when exposed to high interstitial fluid glucose concentration in the capillary networks,[14] thereby releasing insulin for quick uptake through the regional capillary vessels and lymph networks to subsequently regulate BGLs.[14]

RESULTS AND DISCUSSION

TSPBA was synthesized using quaternization reaction of N^1,N^1,N^3,N^3-tetramethylpropane-1,3-diamine in the presence of excess 4-(bromomethyl)phenylboronic acid (Scheme S1). The quaternary ammonium groups on TSPBA significantly enhanced its water solubility (~100 mg/mL), which facilitates the gel formation with PVA aqueous solution without organic solvents. Upon oxidation in the presence of 10 mM H_2O_2, 70% of TSPBA released p-quinone methide (p-hydroxylmethylene-phenol) and became tertiary amines in 1 has demonstrated by 1H NMR (Figure S2).[35] Insulin-NBC was prepared in the presence of a slight excess of NBC in a mixed solvent composed of DMSO and 10 mM $NaHCO_3$ aqueous solution.[36] The product was purified using preparative scale high-performance liquid chromatography (HPLC)[22] and was confirmed by molecular weight to be a conjugate of one insulin modified by one NBC using MALDI-TOF mass spectroscopy (Figure S3). Importantly, insulin-NBC had much higher aqueous solubility (>100 mg/mL) at pH 7.4 than native insulin, which was critical to prepare MN gels with a high loading capacity of insulin. The phenylboronic ester of insulin-NBC can be hydrolyzed in an aqueous solution; this reaction is facilitated in the presence of diols.[36] The insulin-NBC could then be conjugated to PVA chains *via* the kinetic ester bond between the phenylboronic acid and the *cis*-1,3-diol in PVA.[38] Addition of TSPBA to this reaction solution led to a rapid increase in the elastic (*G'*) modulus and formation of a network between the PVA chains in 60 s (Figure S4).[39] The gelation of PVA by TSPBA is critical for maintaining the integrity of the shell structure, which is composed of water-sensitive materials, and specifically prevents its dissolution to aqueous solution when preparing the core.

The H_2O_2-sensitive insulin release was evaluated in the presence of 10 mM H_2O_2 in PBS at pH 7.4. Insulin was released from a formed gel with the addition of H_2O_2 at a steady rate, and more than half of insulin was released within 2 h (Figure 2a). Although the esters between phenylboronic acids and diols are generally unstable in acidic solution,[40] the gel formed between PVA and phenylboronic acid is stable in the acidic environment.[38] At pH 3.5, the gel showed high stability, and insulin was released at a rather slow rate as compared to that at pH 7.4.

Next, the release rate of insulin was assessed in the presence of GOx in PBS at initial pH 7.4 at three different glucose concentrations, including a typical hyperglycemic level (400 mg/dL), a normoglycemic level (100 mg/dL), and a control level (0 mg/dL). The H_2O_2 generation rate was measured using a fluorometric hydrogen peroxide assay kit.[41] At the hyper-glycemic glucose concentration of 400 mg/dL, H_2O_2 generation was efficient and reached as high as 6 mM within 60 min (Figure 2b). Compared to the hyperglycemic solution, H_2O_2 was generated at a much slower rate in the normoglycemic solution of 100 mg/dL glucose. The insulin release corresponded to the H_2O_2 release such that the insulin release rate was dramatically promoted under a glucose concentration of 400 mg/dL compared to that of 100 mg/ dL, whereas negligible insulin release was observed when the gel was incubated in the control solution (Figure 2c), consistent with the morphology change of gels (Figure 2d).

Moreover, the release rate of insulin from PVA-TSPBA gels was steadily enhanced when gradually increasing the glucose concentrations of the tested solutions from normoglycemic to hyperglycemic conditions, where a maximum of a 15-fold difference in insulin release rate was achieved in 2 h when the glucose concentration was increased from 100 to 400 mg/dL (Figure 2e). The limited release of insulin at normoglycemia is a significant safety feature for the *in vivo* application. Additionally, a pulsatile kinetic release profile of insulin was monitored for several cycles by alternately varying glucose concentrations between normoglycemic and hyperglycemic conditions, and the pulsatile release profile of insulin was achieved when the gels were alternately exposed to the normal and hyperglycemic levels (Figure 2f). In sum, these findings suggest that the dissociation of cross-linked gels only takes place under hyperglycemic conditions, and the PVA-TSPBA gels release insulin in a glucose concentration-dependent behavior. Finally, the far-UV circular dichroism (CD) spectra of the native and released insulin from gels (1 mg/mL) were similar, suggesting that released insulin retains α-helical secondary structure and bioactivity (Figure S5).

To fabricate the core–shell MN gel, PVA-TSPBA gels were integrated into MN array patch using a micromolding approach.[14] We developed a “solution-gelation” method to conveniently load the cross-linked gel into MNs and form a core–shell structure. Briefly, diluted aqueous solutions of PVA, TSPBA, and CAT-NG (Figure S6) with low viscosity were prepared, combined, and deposited in a silicone mold. The mixed solution was kept in the mold under vacuum for 30 min and then centrifuged at 500 rpm for 1 h to form a “shell” on the mold. Another round of diluted aqueous solutions of PVA, insulin-NBC, TSPBA, and GO**x**-NG (Figure S7) were loaded into the mold, and this procedure was repeated for several times until a predetermined amount of insulin-loaded gel was achieved. During this process, methacrylated PVA and radical initiator were added to the native PVA aqueous solution to form a partially nondegradable network. Finally, hyaluronic acid (HA) aqueous solution was cast and dried under vacuum to provide a base for the mechanical support.[14] The resulting device was arranged in a 20 × 20 MN array on a 12 × 12 mm^2 patch. The needle had a conical shape with a base diameter of 300 μm, 5 μm at the tip, and a height of 600 μm (Figure 3a). The structure of MNs was confirmed by SEM and fluorescence microscopy (Figure 3b–c). The mechanical strength of MN was determined as 2 N/needle (Figure 3d), which sufficiently allows for skin insertion without breaking.[42,43] To validate the feasibility of coating a CAT layer on MN arrays, a hollow MN array patch constructed by rhodamine B labeled CAT-NG-loaded PVA-TSPBA gel shell was prepared. These hollow MNs showed a complete shell structure in a bottom view, side view, or overhead view (Figure 3e; Figure S8). In addition, we found that the integrity of this CAT-NG-loaded shell was not affected when preparing the core part (Figure 3f). Collectively, these results demonstrated the feasibility of preparing a core-shell MN array, with a core loaded with insulin and GO**x**-NG, in addition to a shell embedded with CAT-NG. The methacrylated PVA formed gel was shown to selectively release insulin over GO**x**-NG (Figure 3g; Figure S9). Release of GO**x**-NG was likely prevented due to its much larger size (~12 nm) than insulin, thereby reducing the potential local and systemic toxicity of GO**x**.31

The *in vivo* performance of the core–shell MN array patches was evaluated in a mouse model of type 1 diabetes induced by streptozotocin (STZ). The mice were divided into six groups: (1) treatment with CAT-NG shelled MN array patch of GO**x**-NG and insulin-NBC-

loaded gels (MN-CAT); (2) treatment with subcutaneous injection of human recombinant insulin; (3) treatment with MN array patch of GO**x**-NG and insulin-NBC-loaded gels (MN-Gel(G+I)) without a shell; (4) treatment with MN array patch only loaded with blank gel (MN-Gel); (5) treatment with MN array patch of insulin-NBC-loaded gels (MN-Gel(I)); and (6) treatment with MN array patch of GO**x**-NG, insulin-NBC, and CAT-NG-loaded gels (MN-Gel(G+C +I)). The insulin dosage was set at 50 mg/kg for all MN-based insulin treatments. Staining by trypan blue indicated successful penetration of MNs in the excised skin (Figure 4a-b).[44] In addition, the temporal microchannels on the skin caused by MNs recovered quickly within 2 h post-treatment (Figure S10).

BGLs of the mice were monitored over time following administration. A rapid decrease of BGLs of mice treated by MN-Gel(G+I) (Figure S11) and MN-CAT (Figure 4c) was observed in 30 min post-administration, and no significant difference has been observed between these two groups, indicating that CAT shell does not affect the local concentration of H_2O_2 in the MN core. The BGLs then slowly decreased to around 100 mg/dL and maintained near 200 mg/ dL for almost 6 h, much longer than subcutaneously injected insulin (Figure 4c). This was attributed to the quick local generation of H_2O_2 through the oxidation of glucose in the presence of GO**x** as well as the high sensitivity of gel to H_2O_2. In contrast, no obvious BGLs reduction was observed for the mice treated with MN-Gel(I), MN-Gel (G+C+I), and MN-Gel. These results were consistent to that observed in diabetic mice subcutaneously injected with PVA-TSPBA gel with or without GO**x** (Figure S12). Taken together, these observations confirmed the essential role of H_2O_2 in releasing insulin as well as the high stability of insulin-NBC in PVA-TSPBA gel in the physiological environment. *In vitro*, CAT can preferentially decompose H_2O_2 efficiently at normoglycemia (100 mg/dL) (Figure S13). However, the capability of MN-Gel(G+C+I) to reduce BGLs was significantly inhibited because limited insulin can be released from MN due to the *in situ* exhaustion of H_2O_2 in the presence of CAT in the MN core even under a hyperglycemic condition (Figure 4c), suggesting the necessity to separate CAT in a shell part to establish a robust level of H_2O_2 in the core part locally. Additionally, the plasma human insulin levels in mice treated with MN-CAT and MN-Gel(G+I) were significantly higher than those treated with MN-Gel(I) (Figure S14).

Intraperitoneal glucose tolerance tests (IPGTTs) were further carried out 1 h post-administration of MNs or insulin. A spike in BGLs was observed for all groups after the IPGTT (Figure 4d). However, only healthy mice and MN-CAT could restore blood glucose levels to a normoglycemic level within a short period, and the mice treated with MN-CAT showed significantly enhanced glucose tolerance to the glucose challenge (Figure 4e). In order to assess the risk of hypoglycemia associated with treatment by MN-CAT, the BGLs of healthy mice treated with MN array patch were observed. The BGLs of mice treated with insulin showed a remarkable decrease, while the BGLs of mice treated with MN-CAT showed only a slight decrease, consistent with the slow release of insulin from gels under normoglycemic state (Figure 4f). Additionally, the MN-CAT treated group showed significantly lower hypoglycemia index than insulin (Figure 4g), suggesting that the MN-CAT is safe for clinical application. Furthermore, a 40-hour-long consecutive MN administration was performed to evaluate the *in vivo* glucose control capability of MN

(Figure 4h). During this time, BGLs were maintained in a narrow range between 100 and 250 mg/dL, and critically, no hypoglycemia was recorded.

The reaction between the phenylboronic acid and H_2O_2 alleviates the harm of generated H_2O_2 to surrounding tissues. However, any excessive unreacted H_2O_2 still carries the potential to be harmful. Compared to the skin treated with MN-Gel (Figure 5a), apparent inflammation was observed for mice treated with MN-Gel(G+I). A similar phenomenon was observed for skins treated with directly subcutaneously injected gel (Figure S15). In sharp contrast, almost no visible inflammation was observed on skins of mice treated with MN-CAT and MN-Gel(G+C+I) (Figure 5a). These findings were reinforced in hematoxylin and eosin (H&E) staining results. Compared with skin treated with MN-Gel, skin samples treated with MN-Gel(G+I) showed obvious neutrophil infiltration, indicating a pathophysiological response and tissue damage induced by the generated H_2O_2.[45] However, substantially reduced neutrophil infiltration was observed in the skin of mice treated with MN-Gel(G+C+I) and MN-CAT. The epidermal thickness and skin thickness for mice treated with both MN-CAT and MN-Gel(G+C+I) were comparable to that of skin treated with blank MN but significantly thinner than they were for mice treated with MN-Gel(G+I) (Figure 5b).[46] Moreover, the skin tissue stained with the *in situ* terminal deoxynucleotidyl transferase dUTP nick end labeling (TUNEL) assay clearly demonstrated the cell apoptosis in the skin sample treated with MN-Gel(G+I), whereas negligible cell death was observed in the skin tissue treated with CAT-loaded or coated MNs (Figure 5c).

CONCLUSIONS

In summary, we demonstrated a core–shell gelated MN-array patch for glucose-responsive smart insulin delivery. The MN-Gels were prepared *via* a “solution-gelation” method involving layer-by-layer deposition of the diluted solution. *In vitro* experiments showed that this cross-linked gel could rapidly release insulin when triggered by GO**x**-generated H_2O_2 under hyperglycemic conditions. Elevated local levels of H_2O_2 promote detachment of insulin from the gel matrix and degradation of the matrix itself, which contributes to the efficient glucose responsiveness. *In vivo* experiments indicated that the MN-CAT was highly effective in regulating BGLs and maintaining normoglycemia while avoiding the critical risk of hypoglycemia. Importantly, utilization of CAT coating shows significant promise to eliminate the inflammation caused by the generated H_2O_2. This bioresponsive core–shell MN array patch offers a platform technique for transdermal drug delivery in a physiological factor-controlled manner and enhanced biocompatibility.[47–50]

METHODS

H_2O_2 Generation Rate Assay in Glucose Solution in the Presence of GOx.

The H_2O_2 concentration was determined using a fluorometric hydrogen peroxide assay kit according to the manufacturer’s protocol (Sigma-Aldrich). Glucose solutions (100 or 400 mg/dL) containing GO**x** (0.2 mg/mL) were incubated at 37 °C. Samples (10 μL each tube) were withdrawn and diluted at timed intervals, and the fluorescence intensity was detected.

Preparation of Insulin-NBC-Loaded PVA-TSPBA Gel.

PVA-TSPBA gel was prepared by mixing PVA and TSPBA. PVA (10 wt % in H_2O, 100 μL) and insulin-NBC (10 wt % in H_2O, 30 μL) were mixed first, followed by the addition of TSPBA (10 wt % in H_2O, 30 μL) to fabricate a tough gel. During the in vitro insulin release experiment, this gel was cut into pieces and incubated under different conditions.

In Vitro Insulin Release from PVA-TSPBA Gels.

Insulin-NBC-loaded PVA-TSPBA gels were equally divided into centrifuge tubes containing 1 mL 10 mM PBS at pH 7.4. Various amounts of glucose (0, 100, or 400 mg/dL final concentration) and GOx (0.2 mg/mL) were added to the solution. At predetermined time intervals, solution (10 μL each tube) was withdrawn and stained with Coomassie blue (200 μL), and the absorbance at 595 nm was detected on an Infinite 200 PRO multimode plate reader (Tecan Group Ltd.). The insulin concentration was calibrated by a standard curve.

Fabrication of Microneedle Array Patch (with MN-CAT as an Example).

MNs used in this study were prepared *via* five silicone molds purchased from Blueacre Technology Ltd. Each MN had a round base of 300 μm in diameter, which tapers over a height of 600 μm to a tip radius of around 5 μm. The MNs were arranged in a 20 × 20 array with 600 μm tip–tip spacing. First, diluted aqueous solutions of PVA (3.5 wt % in H_2O, 450 μL), TSPBA (3.5 wt % in H_2O, 150 μL), and CAT-NG (1 mg in 400 μL H_2O) were prepared and mixed. After deposition in a silicone mold, the solution was kept under reduced vacuum for 30 min and then transferred to a Hettich Universal 32R centrifuge for 20 min at 500 rpm to compact gel solution into MN cavities to form a membrane on the mold. Then, diluted aqueous solutions of PVA, methacrylated PVA, TSPBA, GOx-NG, and photoinitiator (Irgacure 2959; 5 wt %/vol) were loaded into mold, and this procedure was repeated for several times until predetermined amounts of insulin-NBC gel were loaded. Finally, 2 mL HA (4 wt % in H_2O) was filled in each micromold surrounded by silver adhesive tape and dried under vacuum for 2 days. After the desiccation, the MN array patches were separated from the silicone molds carefully and exposed to UV irradiation (wavelength of 365 nm) for a short period for cross-linking. The morphology of the MNs was characterized using an FEI Verios 460L field-emission scanning electron microscope.

In Vivo Studies Using Streptozotocin-Induced Diabetic Mice.

The *in vivo* efficacy of both MN-array patches and gels for diabetes treatment was evaluated on streptozotocin-induced adult diabetic mice (male C57B6, age 8 wk; Jackson Laboratory). The animal study protocol was approved by the Institutional Animal Care and Use Committee at North Carolina State University and the University of North Carolina at Chapel Hill. MN array patch was pressed firmly for the first 5 s, during which the shape and mechanical strength of MN were maintained for easy penetration through the epidermis, and pressed softly for additional 2 min to make MN absorb the liquid. The plasma glucose was measured from tail vein blood samples (~3 μL) of mice using the Clarity GL2Plus glucose meter (Clarity Diagnostics). Mouse glucose levels were monitored for 2 days before drug administration. Five mice for each group were selected to be treated using MN or native insulin. The glucose level of each mouse was monitored until stabilization. For mice treated

with insulin-NBC-loaded gels, PVA (10 wt % in H_2O), insulin-NBC (50 μg in 10 μL H_2O), GOx-NG (3 μg in 5 μL H_2O), and TSPBA (10wt% in H_2O) were consecutively injected subcutaneously to form the gel *in situ*.

Statistical Analysis

Differences in blood glucose levels between the treated groups and controlled groups were determined by unpaired Student's *t*-test. The results were considered statistically significant if the two-tailed *P*-values were <0.05. The statistical approach remained consistent throughout all analyses.

Supplementary Material

Refer to Web version on PubMed Central for supplementary material.

ACKNOWLEDGMENTS

This work was supported by grants from the American Diabetes Association (grant no. 1–15-ACE-21), National Science Foundation (grant no. 1708620), Alfred P. Sloan Foundation (Sloan Research Fellowship), and NC TraCS, NIH's Clinical and Translational Science Award (CTSA, grant no. 1UL1TR001111) to Z.G. This work was performed in part at the Analytical Instrumentation Facility (AIF) at North Carolina State University, which is supported by the State of North Carolina and the National Science Foundation (grant no. 1542015). The AIF is a member of the North Carolina Research Triangle Nanotechnology Network (RTNN), a site in the National Nanotechnology Coordinated Infrastructure (NNCI).

REFERENCES

(1). Mo R, Jiang T, Di J, Tai W, Gu Z. Emerging Micro- and Nanotechnology Based Synthetic Approaches for Insulin Delivery Chem. Soc. Rev. 2014; 43:3595–3629. [PubMed: 24626293]

(2). Veiseh O, Tang BC, Whitehead KA, Anderson DG, Langer R. Managing Diabetes with Nanomedicine: Challenges and Opportunities Nat. Rev. Drug Discovery. 2015; 14:45–57. [PubMed: 25430866]

(3). Ohkubo Y, Kishikawa H, Araki E, Miyata T, Isami S, Motoyoshi S, Kojima Y, Furuyoshi N, Shichiri M. Intensive Insulin Therapy Prevents the Progression of Diabetic Microvascular Complications in Japanese Patients with Non-Insulin-Dependent Diabetes Mellitus: A Randomized Prospective 6-Year Study Diabetes Res. Clin. Pract. 1995; 28:103–117. [PubMed: 7587918]

(4). Owens DR, Zinman B, Bolli GB. Insulins Today and Beyond Lancet. 2001; 358:739–746. [PubMed: 11551598]

(5). Cengiz E, Sherr JL, Weinzimer SA, Tamborlane WV. New-Generation Diabetes Management: Glucose Sensor-Augmented Insulin Pump Therapy Expert Rev. Med. Devices. 2011; 8:449–458. [PubMed: 21728731]

(6). Bequette BW. A Critical Assessment of Algorithms and Challenges in the Development of a Closed-Loop Artificial Pancreas Diabetes Technol. Ther. 2005; 7:28–47. [PubMed: 15738702]

(7). Bratlie KM, York RL, Invernale MA, Langer R, Anderson DG. Materials for Diabetes Therapeutics Adv. Healthcare Mater. 2012; 1:267–284.

(8). Gordijo CR, Koulajian K, Shuhendler AJ, Bonifacio LD, Huang HY, Chiang S, Ozin GA, Giacca A, Wu XY. Nanotechnology-Enabled Closed Loop Insulin Delivery Device: In Vitro and in Vivo Evaluation of Glucose-Regulated Insulin Release for Diabetes Control Adv. Funct. Mater. 2011; 21:73–82.

(9). Gu Z, Aimetti AA, Wang Q, Dang TT, Zhang Y, Veiseh O, Cheng H, Langer RS, Anderson DG. Injectable NanoNetwork for Glucose-Mediated Insulin Delivery ACS Nano. 2013; 7:4194–4201. [PubMed: 23638642]

(10). Gu Z, Dang TT, Ma M, Tang BC, Cheng H, Jiang S, Dong Y, Zhang Y, Anderson DG. Glucose-Responsive Microgels Integrated with Enzyme Nanocapsules for Closed-Loop Insulin Delivery ACS Nano. 2013; 7:6758–6766. [PubMed: 23834678]

(11). Hassan CM, Doyle FJ, Peppas NA. Dynamic Behavior of Glucose-Responsive Poly(Methacrylic Acid-g-Ethylene Glycol) Hydrogels Macromolecules. 1997; 30:6166–6173.

(12). Yu J, Zhang Y, Bomba H, Gu Z. Stimuli-Responsive Delivery of Therapeutics for Diabetes Treatment. Bioeng Transl Med. 2016; 1:323–337.

(13). Bakh NA, Cortinas AB, Weiss MA, Langer RS, Anderson DG, Gu Z, Dutta S, Strano MS. Glucose-Responsive Insulin by Molecular and Physical Design Nat. Chem. 2017; 9:937–943. [PubMed: 28937662]

(14). Yu J, Zhang Y, Ye Y, DiSanto R, Sun W, Ranson D, Ligler FS, Buse JB, Gu Z. Microneedle-Array Patches Loaded with Hypoxia-Sensitive Vesicles Provide Fast Glucose-Responsive Insulin Delivery Proc. Natl. Acad. Sci U. S. A. 2015; 112:8260–8265. [PubMed: 26100900]

(15). Tai W, Mo R, Di J, Subramanian V, Gu X, Buse JB, Gu Z. Bio-Inspired Synthetic Nanovesicles for Glucose-Responsive Release of Insulin Biomacromolecules. 2014; 15:3495–3502. [PubMed: 25268758]

(16). Podual K, Doyle FJ III, Peppas NA. Glucose-Sensitivity of Glucose Oxidase-Containing Cationic Copolymer Hydrogels Having Poly(Ethylene Glycol) Grafts J. Controlled Release. 2000; 67:9–17.

(17). Zhang K, Wu XY. Modulated Insulin Permeation across a Glucose-Sensitive Polymeric Composite Membrane J. Controlled Release. 2002; 80:169–178.

(18). Podual K, Doyle FJ, Peppas NA. Preparation and Dynamic Response of Cationic Copolymer Hydrogels Containing Glucose Oxidase Polymer. 2000; 41:3975–3983.

(19). Hu XL, Yu JC, Qian CG, Lu Y, Kahkoska AR, Xie ZG, Jing XB, Buse JB, Gu Z. H2O2-Responsive Vesicles Integrated with Transcutaneous Patches for Glucose-Mediated Insulin Delivery ACS Nano. 2017; 11:613–620. [PubMed: 28051306]

(20). Chen Z, Wang J, Sun W, Archibong E, Kahkoska AR, Zhang X, Lu Y, Ligler FS, Buse JB, Gu Z. Synthetic Beta Cells for Fusion-Mediated Dynamic Insulin Secretion Nat. Chem. Biol. 2018; 14:86–93. [PubMed: 29083418]

(21). Dong Y, Wang W, Veiseh O, Appel EA, Xue K, Webber MJ, Tang BC, Yang X-W, Weir GC, Langer R, Anderson DG. Injectable and Glucose-Responsive Hydrogels Based on Boronic Acid-Glucose Complexation Langmuir. 2016; 32:8743–8747. [PubMed: 27455412]

(22). Chou DH, Webber MJ, Tang BC, Lin AB, Thapa LS, Deng D, Truong JV, Cortinas AB, Langer R, Anderson DG. Glucose-Responsive Insulin Activity by Covalent Modification with Aliphatic Phenylboronic Acid Conjugates Proc. Natl. Acad. Sci. U. S. A. 2015; 112:2401–2406. [PubMed: 25675515]

(23). Matsumoto A, Kurata T, Shiino D, Kataoka K. Swelling and Shrinking Kinetics of Totally Synthetic, Glucose-Responsive Polymer Gel Bearing Phenylborate Derivative as a Glucose-Sensing Moiety Macromolecules. 2004; 37:1502–1510.

(24). Shiino D, Murata Y, Kubo A, Kim YJ, Kataoka K, Koyama Y, Kikuchi A, Yokoyama M, Sakurai Y, Okano T. Amine Containing Phenylboronic Acid Gel for Glucose-Responsive Insulin Release under Physiological pH J. Controlled Release. 1995; 37:269–276.

(25). Matsumoto A, Yoshida R, Kataoka K. Glucose-Responsive Polymer Gel Bearing Phenylborate Derivative as a Glucose-Sensing Moiety Operating at the Physiological pH Biomacromolecules. 2004; 5:1038–1045. [PubMed: 15132698]

(26). Kataoka K, Miyazaki H, Bunya M, Okano T, Sakurai Y. Totally Synthetic Polymer Gels Responding to External Glucose Concentration: Their Preparation and Application to On-Off Regulation of Insulin Release J. Am. Chem. Soc. 1998; 120:12694–12695.

(27). Liu F, Song SC, Mix D, Baudys M, Kim SW. Glucose- Induced Release of Glycosylpoly(Ethylene Glycol) Insulin Bound to a Soluble Conjugate of Concanavalin A Bioconjugate Chem. 1997; 8:664–672.

(28). Joel S, Turner KB, Daunert S. Glucose Recognition Proteins for Glucose Sensing at Physiological Concentrations and Temperatures ACS Chem. Biol. 2014; 9:1595–1602. [PubMed: 24841549]

(29). Wang C, Ye YQ, Sun WJ, Yu JC, Wang JQ, Lawrence DS, Buse JB, Gu Z. Red Blood Cells for Glucose-Responsive Insulin Delivery Adv. Mater. 2017; 29:1606617.

(30). Saravanakumar G, Kim J, Kim WJ. Reactive-Oxygen- Species-Responsive Drug Delivery Systems: Promises and Challenges Adv. Sci. 2017; 4:1600124.

(31). Broom WA, Coulthard CE, Gurd MR, Sharpe ME. Some Pharmacological and Chemotherapeutic Properties of Notatin Br. J. Pharmacol. Chemother. 1946; 1:225–233.

(32). Prausnitz MR. Engineering Microneedle Patches for Vaccination and Drug Delivery to Skin Annu. Rev. Chem. Biomol. Eng. 2017; 8:177–200. [PubMed: 28375775]

(33). Yu J, Zhang Y, Kahkoska AR, Gu Z. Bioresponsive Transcutaneous Patches Curr. Opin. Biotechnol. 2017; 48:28–32. [PubMed: 28292673]

(34). Kitano S, Koyama Y, Kataoka K, Okano T, Sakurai Y. A Novel Drug Delivery System Utilizing a Glucose Responsive Polymer Complex between Poly (Vinyl Alcohol) and Poly (N-Vinyl-2-Pyrrolidone) with a Phenylboronic Acid Moiety J. Controlled Release. 1992; 19:161–170.

(35). Liu X, Xiang J, Zhu D, Jiang L, Zhou Z, Tang J, Liu X, Huang Y, Shen Y. Fusogenic Reactive Oxygen Species Triggered Charge-Reversal Vector for Effective Gene Delivery Adv. Mater. 2016; 28:1743–1752. [PubMed: 26663349]

(36). Wang M, Sun S, Neufeld CI, Perez-Ramirez B, Xu Q. Reactive Oxygen Species-Responsive Protein Modification and Its Intracellular Delivery for Targeted Cancer Therapy Angew. Chem., Int. Ed. 2014; 53:13444–13448.

(37). De Duve C, Baudhuin P. Peroxisomes (Microbodies and Related Particles) Physiol. Rev. 1966; 46:323–357. [PubMed: 5325972]

(38). Piest M, Zhang XL, Trinidad J, Engbersen JFJ. pH-Responsive, Dynamically Restructuring Hydrogels Formed by Reversible Crosslinking of PVA with Phenylboronic Acid Functionalised PPO-PEO-PPO Spacers (Jeffamines (R)) Soft Matter. 2011; 7:11111–11118.

(39). Burns NA, Naclerio MA, Khan SA, Shojaei A, Raghavan SR. Nanodiamond Gels in Nonpolar Media: Colloidal and Rheological Properties J. Rheol. 2014; 58:1599–1614.

(40). Springsteen G, Wang B. A Detailed Examination of Boronic Acid-Diol Complexation Tetrahedron. 2002; 58:5291–5300.

(41). Yamamoto Y, Koma H, Yagami T. Hydrogen Peroxide Mediated the Neurotoxicity of an Antibody against Plasmalemmal Neuronspecific Enolase in Primary Cortical Neurons NeuroToxicology. 2015; 49:86–93. [PubMed: 26038286]

(42). Olatunji O, Das DB, Garland MJ, Belaid L, Donnelly RF. Influence of Array Interspacing on the Force Required for Successful Microneedle Skin Penetration: Theoretical and Practical Approaches J. Pharm. Sci. 2013; 102:1209–1221. [PubMed: 23359221]

(43). Davis SP, Landis BJ, Adams ZH, Allen MG, Prausnitz MR. Insertion of Microneedles into Skin: Measurement and Prediction of Insertion Force and Needle Fracture Force J. Biomech. 2004; 37:1155–1163. [PubMed: 15212920]

(44). Lee IC, He J-S, Tsai M-T, Lin K-C. Fabrication of a Novel Partially Dissolving Polymer Microneedle Patch for Transdermal Drug Delivery J. Mater. Chem. 2015; 3:276–285.

(45). Liu Y, Du J, Yan M, Lau MY, Hu J, Han H, Yang OO, Liang S, Wei W, Wang H, Li J, Zhu X, Shi L, Chen W, Ji C, Lu Y. Biomimetic Enzyme Nanocomplexes and Their Use as Antidotes and Preventive Measures for Alcohol Intoxication Nat. Nanotechnol. 2013; 8:187–192. [PubMed: 23416793]

(46). Jin XJ, Kim EJ, Oh IK, Kim YK, Park CH, Chung JH. Prevention of Uv-Induced Skin Damages by 11,14,17-Eicosatrienoic Acid in Hairless Mice in Vivo J. Korean Med. Sci. 2010; 25:930–937. [PubMed: 20514317]

(47). Sun WJ, Hu QY, Ji WY, Wright G, Gu Z. Leveraging Physiology for Precision Drug Delivery Physiol. Rev. 2017; 97:189–225.

(48). Lu Y, Aimetti AA, Langer R, Gu Z. Bioresponsive Materials Nat. Rev. Mater. 2017; 2:16075.

(49). Peppas NA, Khademhosseini A. Make Better, Safer Biomaterials Nature. 2016; 540:335–336. [PubMed: 27974790]

(50). Ye Y, Yu J, Wen D, Kahkoska AR, Gu Z. Polymeric Microneedles for Transdermal Protein Delivery Adv. Drug Delivery Rev. 2018 10.1016/j.addr.2018.01.015.

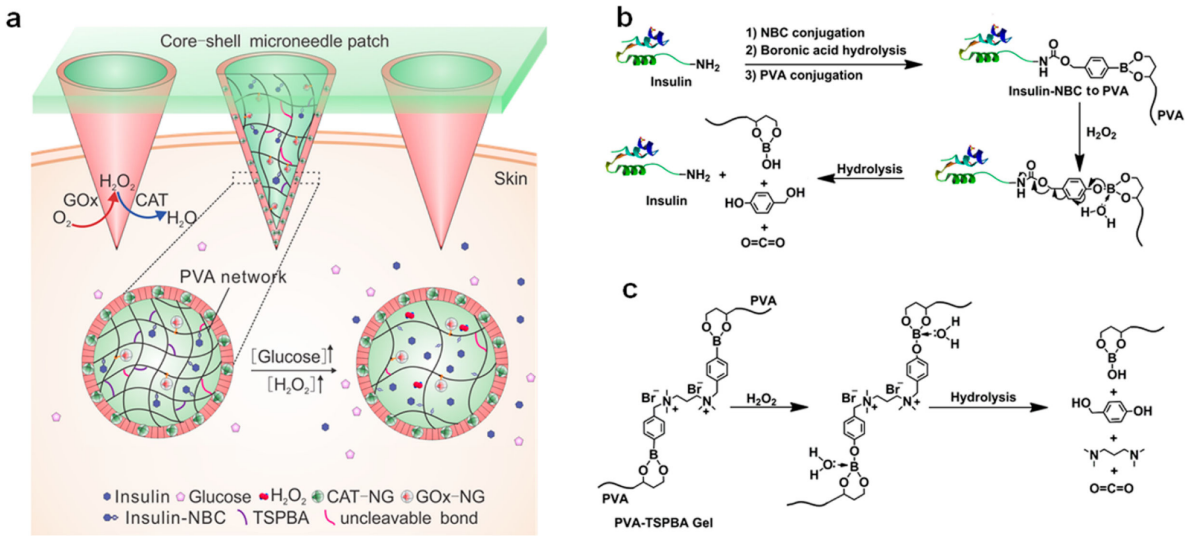

Figure 1.

Schematic representation of the glucose-responsive insulin delivery system using H_2O_2 responsive PVA-TSPBA gel. (a) Insulin is triggered to release by a hyperglycemic state from the core matrix of the PVA-TSPBA MN patch, and the local inflammation can be greatly reduced by the catalase embedded PVA-TSPBA shell. (b) Modification of insulin with NBC and the mechanism of H_2O_2 responsive release. (c) Schematic of the H_2O_2-responsiveness mechanism of PVA-TSPBA gels.

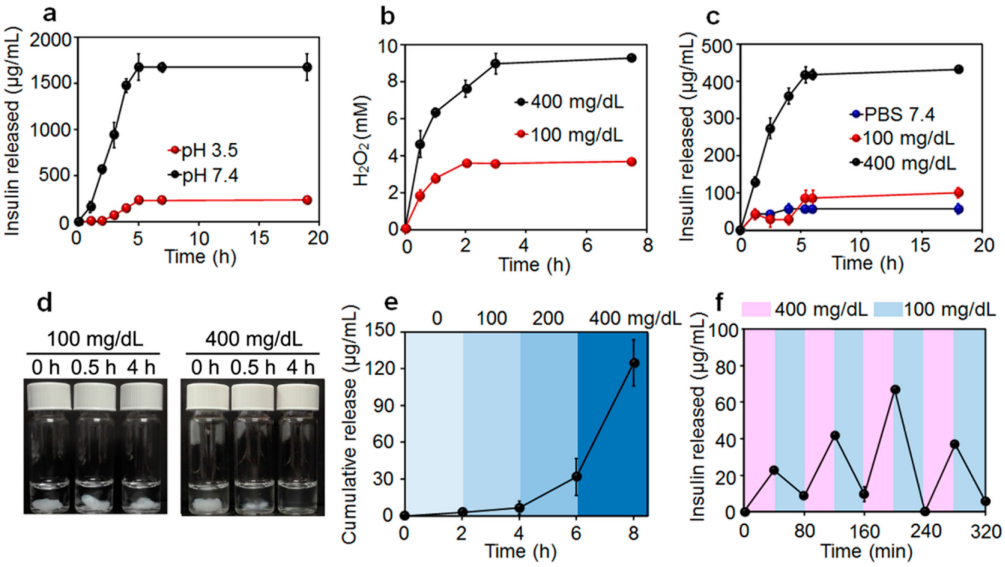

Figure 2.

In vitro glucose-responsive insulin release from PVA-TSPBA gels. (a) Insulin release from PVA-TSPBA gels in PBS with 10 mM H_2O_2 at pH 7.4 and 3.5. (b) Glucose concentration-dependent generation of H_2O_2 in PBS 7.4 in the presence of GOx (0.2 mg/mL). (c) Glucose concentration-dependent insulin release from gels in PBS 7.4 in the presence of GOx (0.2 mg/mL). The glucose concentration was set as 0, 100, and 400 mg/dL. (d) the glucose concentration-dependent morphology changes of gels in PBS 7.4 with GOx (0.2 mg/mL). (e) Self-regulated insulin release profile as a function of glucose concentration. (f) Pulsatile insulin release profile as a function of glucose concentrations over time. Data points represent mean ± SD (n = 3). Error bars indicate SD.

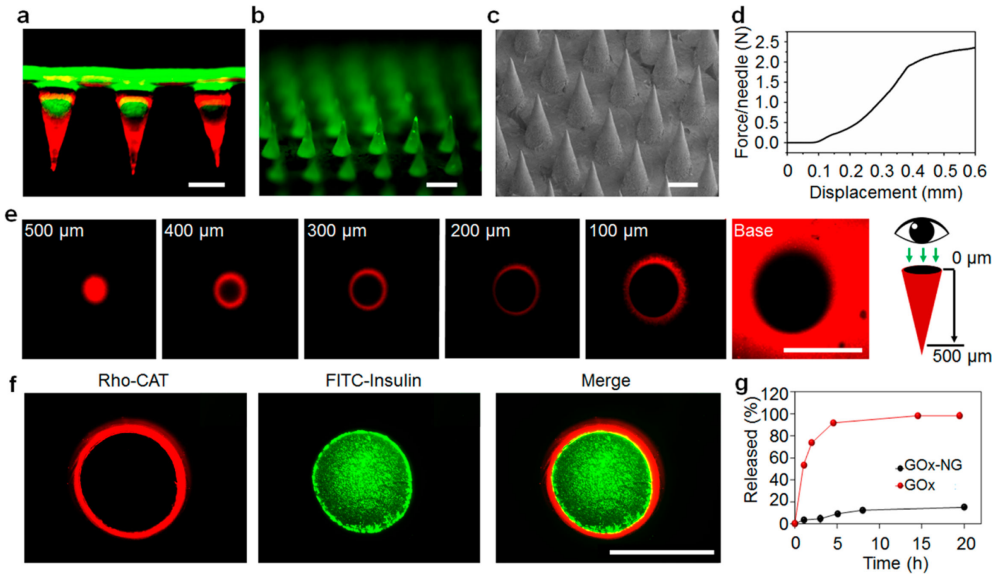

Figure 3.

Characterization of MN array patch of PVA-TSPBA. (a) Representative fluorescence microscopy images of insulin-loaded MN arrays with HA base. Rhodamine B labeled insulin was loaded in PVA-TSPBA gel at the top of MNs (red), while the HA base (green, labeled by FITC-insulin) was mainly located at the bottom. (b) Representative fluorescence image of MN array patch loaded with insulin-FITC. Scale bars, 500 μm. (c) Representative scanning electron microscopy image of MN patch. Scale bar, 300 μm. (d) Mechanical strength of MNs. (e) Representative images of a bottom view of hollow CAT-loaded MNs. These images were obtained using confocal laser scanning microscopy, and the intervals at z-direction were set as 100 μm. Scale bar, 300 μm. (f) Representative images of a cross-section of core–shell MN using cryosection: rhodamine B labeled CAT shell (red), FITC labeled insulin (green), and their overlap. The shell was 25 μm thick as analyzed using software ImageJ. Scale bar, 300 μm. (g) The time-dependent release of GOx or GOx-NG from PVA methacrylate gel.

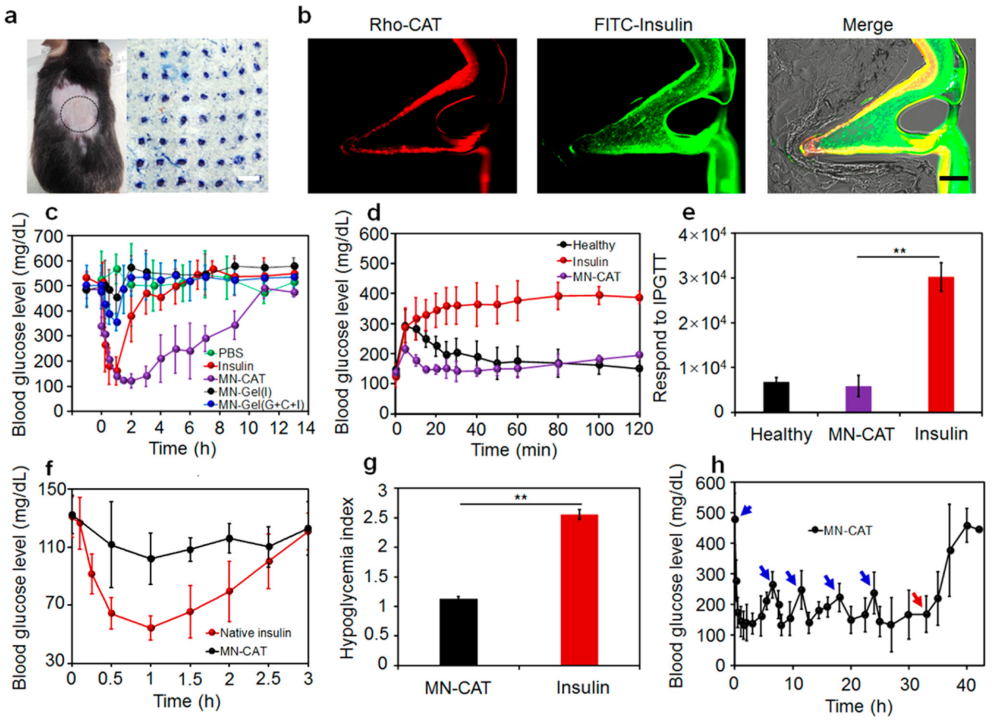

Figure 4.

In vivo evaluation of MN array patches for type 1 diabetes treatment. (a) Mice treated with a MN array patch (left), and the skin inserted by MN array patch was excised and stained using trypan blue (right). Scale bar, 600 μm. (b) Representative images of core–shell MNs inserted into skins: the shell embedding rhodamine B labeled CAT (red), the core labeled by insulin-FITC (green), and their overlap. Scale bar, 100 μm. (c) Blood glucose levels of type 1 diabetic mice treated with different kinds of MN array patches. (d) *In vivo* glucose tolerance test toward diabetic mice at 1 h post-treatment of MN-CAT or subcutaneously injected with insulin. Healthy mice were used as the control. (e) Responsiveness was calculated based on the area under the curve (AUC) in 120 min, with the baseline set at the 0 min blood glucose reading. (f) Blood glucose levels change in healthy mice treated with MN array patch or subcutaneously injected insulin. The treatment was given at 0 min. (g) Quantification of the hypoglycemia index, identified as the difference between the initial and nadir blood glucose readings divided by the time at which nadir was reached. (h) Blood glucose levels change in diabetic mice treated with multiple MN- array patches. The administration of MN-CAT was indicated by blue arrows. Each time, there were two MNs on mice except the first one, and the last two MNs were removed as indicated by red arrows. Student's *t* test: **P < 0.01. Data points represent mean ± SD (n = 5). Error bars indicate SD.

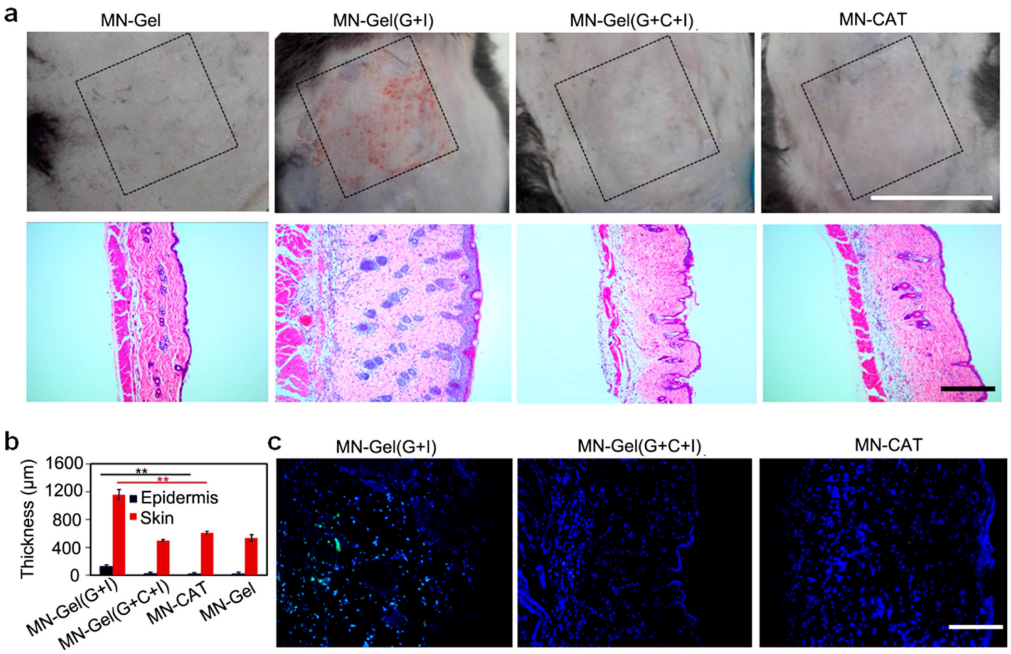

Figure 5.

In vivo biocompatibility studies of MN-CAT arrays for diabetes treatment. (a) Representative images of skins at the treated site of mice and their corresponding H&E staining results. Mice were treated with MN-Gel, MN-Gel(G+I), MN-Gel(G+C+I), and MN-CAT. Scale bars, 1 cm or 300 μm for mice skin images and H&E staining, respectively. (b) Statistical analysis of the thickness of epidermis and skins treated by MNs. The epidermis and skin treated by MN-CAT showed significantly less swelling than that treated with MN-Gel(G+I) (**P < 0.01). Data points represent mean ± SD (n = 3). Error bars indicate SD. (c) Immunohistologic staining with TUNEL assay (green) and Hoechst (blue) of skins treated with MN-Gel(G+I), MN-Gel(G+C+I) and MN-CAT. Scale bars, 150 μm.